International Journal of Solids and Structures 47 (2010) 251–260

Contents lists available at ScienceDirect

International Journal of Solids and Structures

journal homepage: www.elsevier.com/locate/ijsolstr

Analysis of three-dimensional micro-mechanical strain formulations for granular materials: Evaluation of accuracy

O. Durán, N.P. Kruyt *, S. Luding

Department of Mechanical Engineering, University of Twente, The Netherlands

ARTICLE INFO

Article history:
Received 4 March 2009
Received in revised form 25 September 2009
Available online 8 October 2009

Keywords:
Granular materials
Micromechanics
Strain tensor

ABSTRACT

An important objective of recent research on micro-mechanics of granular materials is to develop macroscopic constitutive relations in terms of micro-mechanical quantities at inter-particle contacts. Although the micro-mechanical formulation of the stress tensor is well established, the corresponding formulation for the strain tensor has proven to be much more evasive, still being the subject of much discussion. In this paper, we study various micro-mechanical strain formulations for three-dimensional granular assemblies, following the work of Bagi in two dimensions (Bagi, 2006). All of these formulations are either based on an equivalent continuum approach, or follow the best-fit approach. Their accuracy is evaluated by comparing their results, using data from Discrete Element Method simulations on periodic assemblies, to the macroscopic deformation. It is found that Bagi's formulation (Bagi, 1996), which is based on the Delaunay tessellation of space, is the most accurate. Furthermore, the best-fit formulation based on particle displacements only did unexpectedly well, in contrast to previously reported results for two-dimensional assemblies.

1. Introduction

The constitutive relations that describe the interplay between stress and strain increments in quasi-static deformation of granular materials are very important in many branches of science and engineering, such as in soil mechanics and geophysics. Usually, such constitutive relations are based on experimental observations and are phenomenological in nature. An alternative approach is the micro-mechanical (or multi-scale) approach, in which an objective is to formulate relations between microscopic characteristics of the particles that form the granular assembly and macroscopic continuum characteristics. Thus, the micro-mechanical approach in principle allows to account for the discrete nature of granular materials.

An important component of this approach is the conversion of discrete information at the contact level, such as forces and deformations at contacts, into macroscopic continuum quantities, like stress and strain. The formulation for the average stress tensor (for example Drescher and de Josselin de Jong, 1972; Bagi, 1996) as a sum over all contacts involving the contact force and one additional geometrical quantity (the branch vector), is well established. An alternative formulation is given by Goldhirsch and Goldenberg (2005).

The analogous formulation for the average displacement gradient, in terms of the relative displacement between particles in contact and associated geometrical quantities (Bagi, 1996; Kruyt and Rothenburg, 1996; Liao et al., 1997; Satake, 2002, 2004; Kruyt, 2003), has no commonly accepted formulation. In general, the strain formulations can be classified into three groups: based on (1) an equivalent continuum approach (Bagi, 1996; Kruyt and Rothenburg, 1996; Kuhn, 1999; Kruyt, 2003; Tordesillas et al., 2008) or a contact-cell deformation approach (Satake, 2002, 2004), (2) the best fit between the actual particle relative displacements and assumed mean-field displacements determined by the macroscopic strain tensor (Liao et al., 1997; ITASCA, 1999; Cambou et al., 2000) and (3) direct calculation of the velocity gradient from an averaged continuous velocity field (Lätzel et al., 2001; Goldhirsch and Goldenberg, 2005; Luding, 2008a,b). Best-fit strain formulations (2) are attractive due to their simplicity. Although the direct velocity gradient field (3) is simpler to obtain, it averages out the statistical fluctuations of the displacement field.

Recently, Bagi (2006) performed a two-dimensional numerical comparison between various micro-mechanical formulations for the strain tensor, based on an equivalent continuum approach (Bagi, 1996; Kruyt and Rothenburg, 1996; Kruyt, 2003) and the best-fit approach (Liao et al., 1997; Bagi, 2006). When compared to the macroscopic deformation during uni- and biaxial loading, the strain formulations of Bagi (1996) and Kruyt and Rothenburg (1996) were very accurate, with errors close to 1%, whereas the contact-based best-fit strain of Liao et al. (1997) and the Cosserat strain of Kruyt (2003) failed to reproduce the macroscopic

* Corresponding author. Address: Department of Mechanical Engineering, University of Twente, 7500 AE Enschede, The Netherlands. Tel.: +31 53 4892528; fax: +31 53 4893695.
E-mail address: n.p.kruyt@utwente.nl (N.P. Kruyt).

0020-7683/$ - see front matter © 2009 Elsevier Ltd. All rights reserved.
doi:10.1016/j.ijsolstr.2009.09.035

deformation, with errors of about 20% and 10%, respectively (Bagi, 2006). Furthermore, the particle-based best-fit strain, used in the commercial software ITASCA (ITASCA, 1999), had mixed results: for frictionless assemblies, it was very accurate, while for frictional grains it gave errors of 5–20%, depending on the loading state (Bagi, 2006).

Due to its relevance for micro-mechanical investigations, we extend here the previous work of Bagi for the two-dimensional case, to the three-dimensional case. Strain formulations that are investigated here are the equivalent continuum formulation of Bagi (1996), and three best-fit formulations: the particle-based one (ITASCA, 1999), and two modifications made by Cambou et al. (2000) of the contact-based best-fit formulation proposed by Liao et al. (1997). Note that other interesting formulations are not included, either because they are defined only for the two-dimensional case, for instance (Kruyt and Rothenburg, 1996) or because they involve rather high computational costs (Goldhirsch and Goldenberg, 2005; Satake, 2004).

To our knowledge, there is only one similar study for the three-dimensional case (Drummen, 2006), where different strain formulations, in particular, the equivalent continuous strain of Bagi (1996) and Satake (2004) and the particle-based best-fit strain (ITASCA, 1999), are applied to the deformation of a periodic hexagonal close packed (HCP) assembly. For this ideal packing, the three strain formulations reproduce the imposed macroscopic strain with an error of less than 3% (Drummen, 2006). However, this ideal result is not sufficient to demonstrate their accuracy in the more general case of disordered packings. An important difference between the present analysis and previous studies is that boundary effects are excluded here by the use of periodic boundaries.

The outline of this study is as follows: in Section 2, we introduce the different strain formulations. In Section 3, we present Discrete Element Method (DEM) simulations of both isotropic and triaxial compression. Using the DEM simulation results, we compare the micro-mechanical strains with the actual macroscopic deformation in Section 4. Finally, in Section 5, findings are discussed and conclusions presented.

2. Micro-mechanical strain

The strain tensor ϵ_{ij} is defined as the symmetrical part of the continuum-mechanical displacement gradient $\partial u_i/\partial x_j$, where $u_i(x_j)$ is the displacement field with respect to the selected reference configuration. However, for simplicity in the terminology, in the following we will refer to the displacement gradient $(\partial u_i/\partial x_j)$ simply as the strain tensor ϵ_{ij},

$$\epsilon_{ij} \equiv \frac{\partial u_i}{\partial x_j}. \tag{1}$$

Furthermore, as the sign convention for stresses and strains, we will consider compression as negative.

The average $\bar{\epsilon}_{ij}$ of the strain tensor over a volume V, enclosed by the surface S, is given by

$$\bar{\epsilon}_{ij} = \frac{1}{V}\int_V \epsilon_{ij}\,dV = \frac{1}{V}\int_V \frac{\partial u_i}{\partial x_j}\,dV = \frac{1}{V}\int_S u_i n_j\,dS, \tag{2}$$

where the last equality is due to the Gauss theorem and n_j are the components of the outward normal vector to the surface S. Note that the continuum-mechanical displacement field $u_i(x_j)$ is defined over the whole singly-connected domain V. The pore space between the particles of the assembly is averaged out in the homogenisation process, from discrete particle considerations to continuum formulation.

For small and uniform deformations the displacement field, up to linear order in strain, is

$$u_i(\mathbf{x}) = u_i^0 + \bar{\epsilon}_{ij}x_j, \tag{3}$$

where u_i^0 is the displacement of the origin in the reference configuration and a summation over equal subscripts is implied.

2.1. Bagi's equivalent continuum strain

In this section, we will summarize the strain tensor formulation of Bagi (1996). Since this strain formulation is based on the Delaunay tessellation of space, this tessellation is briefly described first. Details of tessellations of space within the context of granular materials are discussed in Bagi (1996, 2006).

The Delaunay tessellation consists of the tessellation of space into simplices, i.e. triangles in the two-dimensional and tetrahedra in the three-dimensional case. Given a set of N points, the simplices defined by the Delaunay tessellation connect the points in such a way that their E edges (connecting lines) are the shortest path between the points. An equivalent definition is that any circle (two dimensions) or sphere (three dimensions) circumscribed around an arbitrary simplex contains no other point. Such a tessellation satisfies the so-called Euler relation between the number of simplices (L), faces (S), edges (E) and vertices $(N): N - E + S - L = 1$ (3D) or $N - E + L = 1$ (2D). Note that the tessellation is such that no gaps or overlaps occur between the simplices.

In a granular system the vertices are chosen to be the centres of the N particles and their edges correspond to the shortest path between them (see Fig. 1). In the sequel only the three-dimensional case of convex particle assemblies is considered.

An edge between particles p and q is geometrically characterized by the branch vector $\mathbf{l}^{pq} \equiv \mathbf{x}^q - \mathbf{x}^p$, where $\mathbf{x}^p$ $(\mathbf{x}^q)$ is the position of particle $p(q)$. For convex particles, the subset C of all edges E, resulting from the Delaunay tessellation, that represents a physical contact between the particles will be called *real* contacts or simply *contacts*. In contrast, the other $E - C$ edges will be called *virtual*

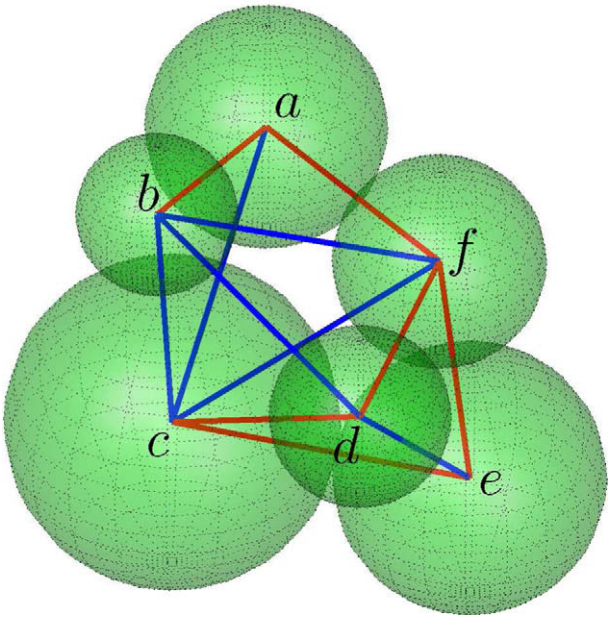

Fig. 1. Delaunay tessellation of a granular system of six spheres of different sizes. The tessellation contains three tetrahedra: $\{a,b,c,f\}$, $\{b,c,d,f\}$ and $\{c,d,e,f\}$. Red edges are contacts, while blue edges indicate *virtual* contacts. (For interpretation of the references to color in this figure legend, the reader is referred to the web version of this paper.)

contacts (Fig. 1). Note that spherical particles are in contact when the distance between their centres is smaller than (or equal to) the sum of their radii.

There are many codes available for performing the Delaunay tessellation (Liu and Snoeyink, 2005). The computational complexity of the tessellation varies between the different codes, being at worst $O(N \log N)$ for efficient implementations.

2.1.1. Strain

Following its continuum definition, the strain tensor for a three-dimensional packing of N particles in a representative volume V can be expressed as the volume average

$$\bar{\epsilon}_{ij} = \frac{1}{V}\sum_L V_L \bar{\epsilon}^L_{ij}, \tag{4}$$

where L runs over all tetrahedra defined by the Delaunay tessellation within the volume $V = \sum_L V_L$ and V_L is the volume of the Lth tetrahedron. The average strain tensor of the Lth tetrahedron $\bar{\epsilon}^L_{ij}$ can be expressed as (Bagi, 1996)

$$\bar{\epsilon}^L_{ij} = \frac{1}{12V_L}\sum_{e(p,q)\in E_L} \Delta u^{pq}_i \left(b^q_j - b^p_j\right), \tag{5}$$

where the sum is over all six edges $e(p,q) \in E_L$ of the Lth tetrahedron. Indices p and q represent the particle at the *tail* and *head* of the directed edge, respectively. The relative displacement at the edge $e(p,q)$ is defined as

$$\Delta \mathbf{u}^{pq} \equiv \mathbf{u}^p - \mathbf{u}^q, \tag{6}$$

where $\mathbf{u}^p$ is the displacement of particle p. For a given tetrahedron L, the vector $\mathbf{b}^p(\mathbf{b}^q)$ represents the outward area-vector of the $p(q)$ face, which is defined as the face opposite to vertex $p(q)$ (see Fig. 2). The norm $|\mathbf{b}^p|$ gives the area of the face.

By collecting the contributions of the various tetrahedra that share the same edge, Eqs. (4) and (5) can be rewritten as an average over the set of edges $\{e\}$ (Bagi, 1996)

$$\bar{\epsilon}_{ij} = \frac{1}{V}\sum_e \Delta u^e_i d^e_j = \frac{E}{V}\left\langle \Delta u^e_i d^e_j \right\rangle_e, \tag{7}$$

where brackets with subscript e represent edge averaging: $\langle\cdot\rangle_e \equiv E^{-1}\sum_e(\cdot)$. The vector $\mathbf{d}^e$ is the complementary area vector of the edge $e(p,q)$, defined as:

$$\mathbf{d}^e \equiv \frac{1}{12}\sum_{t=1}^{T_e}(\mathbf{b}^{q_t} - \mathbf{b}^{p_t}), \tag{8}$$

where the sum is over all T_e tetrahedra that share the edge $e(p,q)$ (Fig. 3). The geometrical meaning of the complementary area vector d^e_i is discussed in Appendix A.

2.1.2. Analogies between the stress and strain formulations

Here, analogies between the micro-mechanical descriptions of strain and stress are emphasized.

Firstly, as was shown before, Bagi's strain $\bar{\epsilon}_{ij}$, Eq. (7) involves the volume average (as a discrete sum over edges) of the relative edge displacement $\Delta\mathbf{u}^e$ and a geometrical quantity $\mathbf{d}^e$. Analogously, the micro-mechanical stress tensor $\bar{\sigma}_{ij}$ can be formulated as a volume average of edge forces $\mathbf{f}^e$ and a geometrical quantity, in this case the branch vectors $\mathbf{l}^e$ (see, for example Bagi, 1996). The micro-mechanical expressions for the average stress and strain tensors are given by

$$\bar{\sigma}_{ij} = \frac{1}{V_\sigma}\sum_e f^e_i l^e_j, \tag{9}$$

$$\bar{\epsilon}_{ij} = \frac{1}{V}\sum_e \Delta u^e_i d^e_j, \tag{10}$$

where V_σ is the summed volume of the Voronoi cells associated with the Delaunay tetrahedra, while V is by definition the summed volume of the Delaunay tetrahedra (Bagi, 1996). However, in the limit of large numbers of particles or for periodic assemblies, both volumes are equal. Therefore, in the sequel we will neglect the distinction between both volumes and consider $V_\sigma = V$.

Furthermore, note that strictly speaking, the stress is averaged over contacts C (the subset of all Delaunay edges that contributes to the force distribution). The $E - C$ *virtual* contacts in the sum do not contribute, since in this case $\mathbf{f}^e = \mathbf{0}$.

Secondly, by pursuing the reverse process, from the macro-scale to the micro-scale, under certain conditions it is possible to estimate the local force and relative displacement at edges from the macroscopic stress and strain, respectively, a process called localization (Cambou et al., 1995). For this process, it is convenient to have a relation between the two geometrical quantities involved in the stress and strain formulation, $\mathbf{d}^e$ and $\mathbf{l}^e$, respectively.

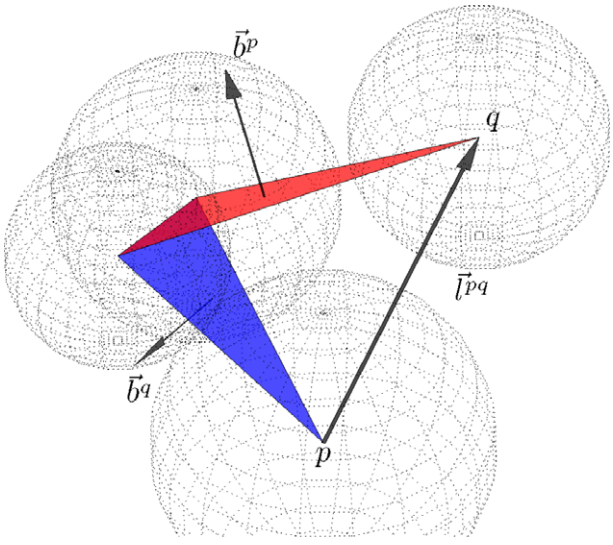

Fig. 2. Sketch of the main quantities corresponding to a tetrahedron containing the edge $e(p,q)$ between particles p (the edge tail) and q (the edge head): the branch vector $\mathbf{l}^{pq} \equiv \mathbf{r}^q - \mathbf{r}^p$ and the area-vector $\mathbf{b}^q$ ($\mathbf{b}^p$) of the face opposite to particle q (p).

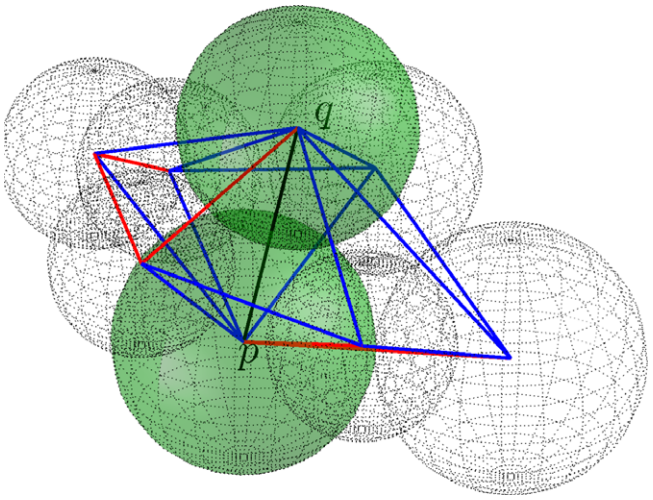

Fig. 3. Tetrahedra that share the edge $e(p,q)$. The tetrahedra are formed by the particles in contact with both p and q (spheres in dashed lines). Red edges are contacts while blue edges indicate *virtual* contacts. (For interpretation of the references to color in this figure legend, the reader is referred to the web version of this paper.)

From their definition, it is possible to show that the surfaces defined by the complementary area vectors $\mathbf{d}^e$ and the generalized branch vectors $\mathbf{l}^e$, determined by the Delaunay tessellation, satisfy the geometrical relation

$$V\delta_{ij} = \sum_e l_i^e d_j^e, \tag{11}$$

where δ_{ij} is the Kronecker delta symbol: 1 if $i = j$ and 0 otherwise.

Using Eq. (11), we can formulate an explicit example of a localization operation. The edge forces and relative displacements are determined from the average stress and strain tensors and $\mathbf{l}^e$ and $\mathbf{d}^e$, by

$$f_i^e = \bar{\sigma}_{ik} d_k^e, \tag{12}$$

$$\Delta u_i^e = \bar{\epsilon}_{ik} l_k^e. \tag{13}$$

This is what we call *uniform stress* and *uniform strain* (see also Kruyt and Rothenburg, 1996). Indeed, after multiplying by l_j^e and d_j^e in Eqs. (12) and (13), respectively, summing over all edges, and substituting Eq. (11), we recover the micro-mechanical stress and strain. Therefore, Eqs. (12) and (13) provide edge forces and relative displacements that are consistent with Eqs. (9) and (10).

In the next section, we will briefly introduce particle-based and contact-based best-fit strains.

2.2. Best-fit strain based on particles

The mean best-fit strain is determined by finding the tensor $\bar{\epsilon}_{ij}$ for which the actual particle displacements most closely match the particle displacements according to Eq. (3) (ITASCA, 1999). Thus, the particle displacement predicted by the average strain $\bar{\epsilon}_{ij}$ is assumed to be

$$u_i^p \approx u_i^0 + \bar{\epsilon}_{ij} x_j^p, \tag{14}$$

with $\bar{\epsilon}_{ij}$ to be determined.

After transforming the particle coordinates x_i^p and the particle displacements u_i^p to new ones, $\tilde{x}_i^p \equiv x_i^p - \langle x_i^p \rangle_p$ and $\tilde{u}_i^p \equiv u_i^p - \langle u_i^p \rangle_p$, relative to the geometrical centre of the assembly $\langle x_i^p \rangle_p$ (here the brackets, $\langle \cdot \rangle_p \equiv N^{-1} \sum_p (\cdot)$, imply an average over all N particles), the constant u_i^0 in Eq. (14) becomes zero, and the shifted particle displacements are assumed to be given by

$$\tilde{u}_i^p \approx \bar{\epsilon}_{ij} \tilde{x}_j^p. \tag{15}$$

The strain tensor $\bar{\epsilon}_{ij}$ is then obtained from a least-squares approach by minimizing the difference between the mean-field relative particle displacement $\left(\bar{\epsilon}_{ij}\tilde{x}_j^p\right)$ and the actual particle displacement $\tilde{u}_i^p$, i.e.

$$\min_{\bar{\epsilon}_{ij}} \sum_p \left(\tilde{u}_i^p - \bar{\epsilon}_{ij}\tilde{x}_j^p\right)\left(\tilde{u}_i^p - \bar{\epsilon}_{ik}\tilde{x}_k^p\right). \tag{16}$$

The solution for $\bar{\epsilon}_{ij}$ is

$$\bar{\epsilon}_{ij} = w_{ik}^{-1} \left\langle \tilde{u}_j^p \tilde{x}_k^p \right\rangle_p, \tag{17}$$

where w_{ik}^{-1} is the inverse of the tensor $w_{ik} \equiv \langle \tilde{x}_i^p \tilde{x}_k^p \rangle_p$. This tensor shows some similarities with a (massless) moment of inertia tensor of the assembly.

2.3. Best-fit strain based on contacts

In a similar way as for the particle-based strain, the contact-based strain, in its original form (Liao and Chan, 1997), is obtained after minimizing the difference between the mean-field contact relative deformation $\bar{\epsilon}_{ij} l_j^c$, that corresponds to uniform strain (where $\mathbf{l}^c$ is the contact branch vector), and the actual δu_i^c. Here, the strain is determined from

$$\min_{\bar{\epsilon}_{ij}} \sum_c \left(\delta u_i^c - \bar{\epsilon}_{ij} l_j^c\right)\left(\delta u_i^c - \bar{\epsilon}_{ik} l_k^c\right), \tag{18}$$

where the sum runs over all contacts $c \in C$.

In contrast to the relative contact displacement Δu_i^c, the relative contact deformation δu_i^c involves not only particle translations, but also particle rotations

$$\begin{aligned}\delta \mathbf{u}^{pq} &= (\mathbf{u}^p + \boldsymbol{\theta}^p \times \mathbf{r}^{pq}) - (\mathbf{u}^q + \boldsymbol{\theta}^q \times \mathbf{r}^{qp}) \\ &= \Delta \mathbf{u}^{pq} + (\boldsymbol{\theta}^p \times \mathbf{r}^{pq} - \boldsymbol{\theta}^q \times \mathbf{r}^{qp}),\end{aligned} \tag{19}$$

where $\mathbf{r}^{pq}$ ($\mathbf{r}^{qp}$) is the vector from the centre of particle p (q) to the contact point with particle q (p), and θ^p (θ^q) is the rotation vector of particle p (q).

The solution of the least-squares problem leads to the strain expression

$$\bar{\epsilon}_{ij} = \mathscr{F}_{ik}^{-1} \left\langle \delta u_j^c l_k^c \right\rangle_c, \tag{20}$$

where $\mathscr{F}_{ik}^{-1}$ is the inverse of the fabric tensor $\mathscr{F}_{ik} \equiv \langle l_i^c l_k^c \rangle_c$. Brackets with the subscript c, $\langle \cdot \rangle_c \equiv C^{-1} \sum_c (\cdot)$, imply an average over all C contacts.

Based on the failure of the original contact-based best-fit strain to reproduce the macroscopic strain, two improved versions have been proposed (Cambou et al., 2000). In the first version, the relative contact deformation $\delta \mathbf{u}^c$ is replaced by the contact relative displacement $\Delta \mathbf{u}^c$, thus eliminating particle rotations from the strain expression, leading to:

$$\bar{\epsilon}_{ij} = \mathscr{F}_{ik}^{-1} \left\langle \Delta u_j^c l_k^c \right\rangle_c. \tag{21}$$

The second improvement is described in the next subsection.

2.4. Best-fit strain based on edges

In their second version (Cambou et al., 2000) extended the sum to edges (E), instead of only contacts (C). Thus

$$\bar{\epsilon}_{ij} = \mathscr{F}_{ik}^{*-1} \left\langle \Delta u_j^e l_k^e \right\rangle_e, \tag{22}$$

where $\mathscr{F}_{ik}^{*} \equiv \langle l_i^e l_k^e \rangle_e$ is an extended fabric tensor and brackets with a subscript e, $\langle \cdot \rangle_e \equiv E^{-1} \sum_e (\cdot)$, imply an average over all E edges of the tessellation.

It is shown in Appendix B that the edge-based best-fit strain is a close approximation of the Bagi strain, Eq. (7), when the complementary area vector $\mathbf{d}^e$ and the branch vector $\mathbf{l}^e$ are co-linear. Therefore, the edge-based best-fit strain is not a completely independent formulation and it is not expected to be more accurate than the Bagi strain.

3. Discrete element simulations

Discrete Element Method simulations (Cundall and Strack, 1979) have been performed to obtain particle displacements under macroscopic isotropic and triaxial loading conditions. These particle displacements are used to evaluate the accuracy of the various strain formulations introduced in the previous section, by comparing them with the macroscopic strain.

The assembly of particles consists of 250,000 spheres with log-normal radii distribution, with standard deviation 0.25, relative to the mean particle radius $\bar{R}$. The initial packing is prepared under isotropic stress σ_0. Its packing density, i.e. the volume occupied by the particles divided by the total assembly volume (including voids), is 0.65. The contact constitutive relation of Cundall and Strack (1979) is used, with interparticle friction coefficient $\mu = 0.5$ and ratio $k_t/k_n = 0.5$, where k_n and k_t are the constant normal and tangential contact stiffnesses, respectively. The interparti-

cle deformations (or 'overlaps') are small, since the non-dimensional stress ratio $\sigma_0 \bar{R}/k_n = 10^{-3}$ is rather small.

Periodic boundary conditions have been employed to avoid wall effects and to suppress the formations of shear bands so that large, relatively homogeneous deformations can be studied. The length of the initial cubic assembly is about 60 times the average particle diameter.

Two loading conditions have been considered, isotropic loading and triaxial loading. For the former, isotropic loading, an isotropic deformation up to 5% is imposed. In the latter case, an axial deformation up to 20% is imposed along the X-axis, while the lateral stresses are kept constant equal to the initial hydrostatic stress σ_0.

The macroscopic deformation of the periodic box is described by the macroscopic incremental strain, defined as

$$\epsilon^w_{ij} \equiv \left(\frac{dL_i}{L_i}\right)\delta_{ij}, \tag{23}$$

where L_i is the actual system length in the i-direction and δ_{ij} is the Kronecker delta tensor. No summation over index i is assumed. The total strain e_{ij} is then obtained by integration of the successive incremental parts ϵ_{ij}, starting from a reference state '0', with corresponding initial system lengths L^0_i. Therefore,

$$e^w_{ij} = \int_0 \epsilon^w_{ij}, \tag{24}$$

$$= \ln\frac{L_i}{L^0_i}\delta_{ij}. \tag{25}$$

For the triaxial loading, Fig. 4 shows the evolution of the total volumetric strain e^w_V as function of the total axial deformation, $e^w_{11} = \ln L_1/L^0_1$, with the characteristic compression-dilation behavior. The volumetric strain is defined as $e^w_V \equiv \mathrm{tr}\, e^w_{ij} = \ln V/V_0$, where V is the actual averaging volume and V_0 is the volume of the initial state. The evolution of the stress ratio q/p, with deviatoric stress $q = (\sigma_{11} - \sigma_{22})/2$ and pressure $p = \mathrm{tr}\,\sigma_{ij}/3$, is also shown in Fig. 4. The smallest volume and the yield stress are reached after about 1 and 2% of axial deformation, respectively.

4. Results

In order to evaluate the accuracy of the different strain formulations, we calculate the micro-mechanical strains $\bar{\epsilon}_{ij}$, given by Eqs. (7), (17), (21) and (22), from the DEM simulation data. Note that, for the Bagi and the edge-based best-fit strains, Eqs. (7) and (22), the three-dimensional Delaunay tessellation needs to be determined. This is done using Qhull.[1] An important drawback is that Qhull cannot handle periodic boundary conditions at present. The non-periodic tessellation of points close to the system boundaries would lead to artificially flat tetrahedra, which do not represent the actual nearest-neighbor topology of the granular assembly. In order to avoid this spurious effect, we perform the tessellation on the whole domain but calculate the strain on an internal volume, that will be called 'reduced' volume, that contains $M \approx 0.9^3$ N particles. The Bagi strain is then calculated by only taking the contributions of internal tetrahedra, using Eqs. (4) and (5), while the different best-fit strains are calculated using those particles, edges or contacts inside the 'reduced' volume. As is shown below, for this internal volume the mean-field strain is already attained with satisfactory accuracy.

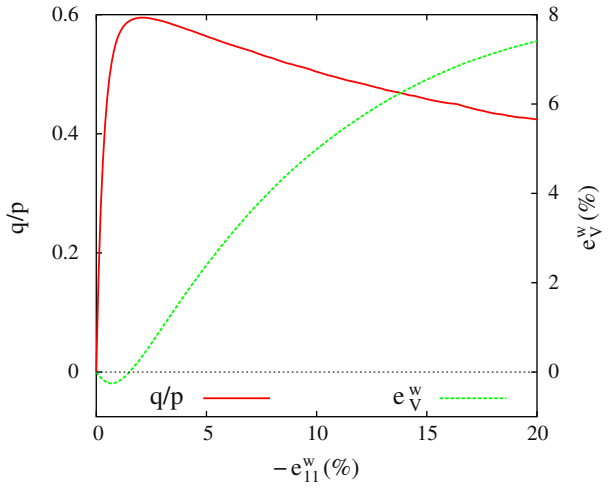

Fig. 4. Triaxial loading: evolution of the total volumetric strain e^w_V and the ratio of the deviatoric stress $q = (\sigma_{11} - \sigma_{22})/2$ to the pressure $p = \mathrm{tr}\,\sigma_{ij}/3$, as a function of the total axial deformation e^w_{11}. Compression is considered as negative.

4.1. Comparison of different strain formulations

We compare Bagi's equivalent continuum and the best-fit strains based on particles, contacts and edges, to the macroscopic strain obtained from the deformation of the periodic box ϵ^w_{ij} Eq. (23). Two loading conditions are considered, isotropic and triaxial compression. In both cases, the comparison is performed at different total axial deformations e^w_{11}, Eq. (25).

For the isotropic compression, the Bagi and particle-based best-fit strains are indistinguishable and very accurate, with deviations around 0.1% (Fig. 5, right), as compared to the contact-based best-fit strain, with deviations above 10%.

In the case of the edge-based best-fit strain, after including the contribution of *virtual* contacts to the overall deformation, the agreement improves (see Fig. 5). Nevertheless, it is still not as accurate as either Bagi or the particle-based strain. This is understandable since, as is shown in Appendix B, the edge-based best-fit strain is an approximation of the Bagi strain.

A similar picture is obtained for the triaxial loading (Figs. 6 and 7). In this case, the strain of Bagi has a small deviation from the macroscopic strain (in the range of 0.1–0.5%), as for isotropic compression. Furthermore, the particle-based best-fit strain is still as accurate as the Bagi strain for describing the internal deformation of a granular system. This differs from the conclusion of a two-dimensional comparison (biaxial test) that showed larger deviations for the former (Bagi, 2006).

Furthermore, from Figs. 6 and 7, it is clear that the contact-based best-fit strain is not able to properly describe the deformation of a granular system. Interestingly, for large axial deformations, the lateral component $\bar{\epsilon}_{22}$ converges to the macroscopic strain, while its maximum deviation is reached for $e^w_{11} \approx 2\%$, where the granular system has its maximum stress ratio q/p (Fig. 4).

Similarly to the isotropic compression case, the edge-based best-fit strain, as the Bagi and the particle-based ones, also reproduces the macroscopic deformation within a few percents deviation, although this deviation increases with the loading $-e^w_{11}$ (Fig. 7).

4.2. Size effect

How close the average strain $\bar{\epsilon}_{ij}$ is to the macroscopic strain ϵ^w_{ij} obviously depends on the size of the averaging volume. It has to be large enough to average out the intrinsic heterogeneity of a granular system.

[1] C-code software developed by the Geometry Center of the University of Minnesota. Qhull is the standard code used by the MATLAB function *delaunayn* (http://www.qhull.org).

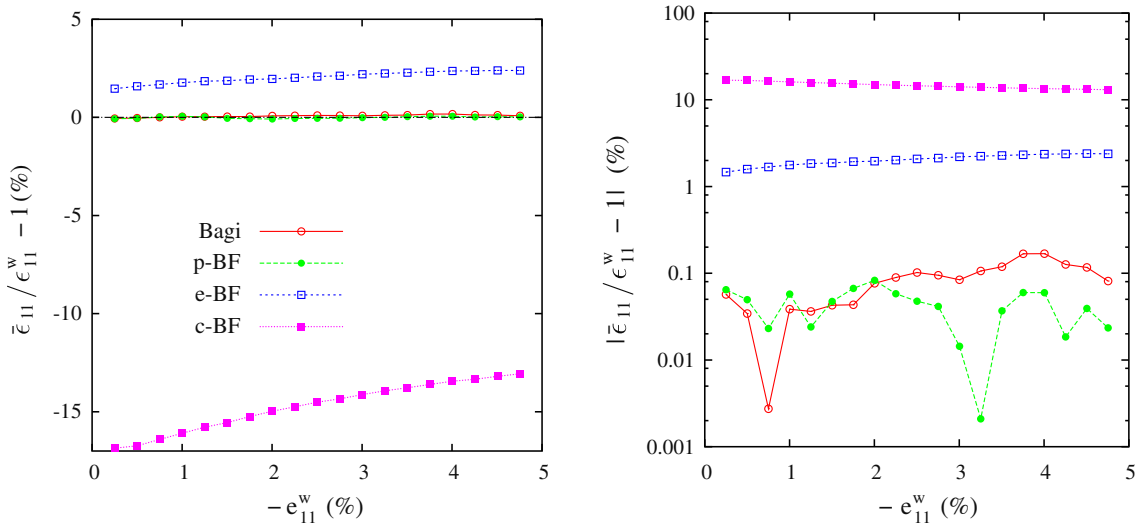

Fig. 5. Isotropic loading: deviation of the axial component $\bar{\epsilon}_{11}$ of the different micro-mechanical strains, from the macroscopic axial strain ϵ^w_{11}, determined from the deformation of the periodic box. p-BF corresponds to the particle-based best-fit strain, e-BF to the edge-based best-fit and c-BF to the contact-based best-fit strain (the same convention is used in similar following figures). Linear scale (left) and semi-log scale (right) are used to clearly identify the scale of the deviations for the different strains.

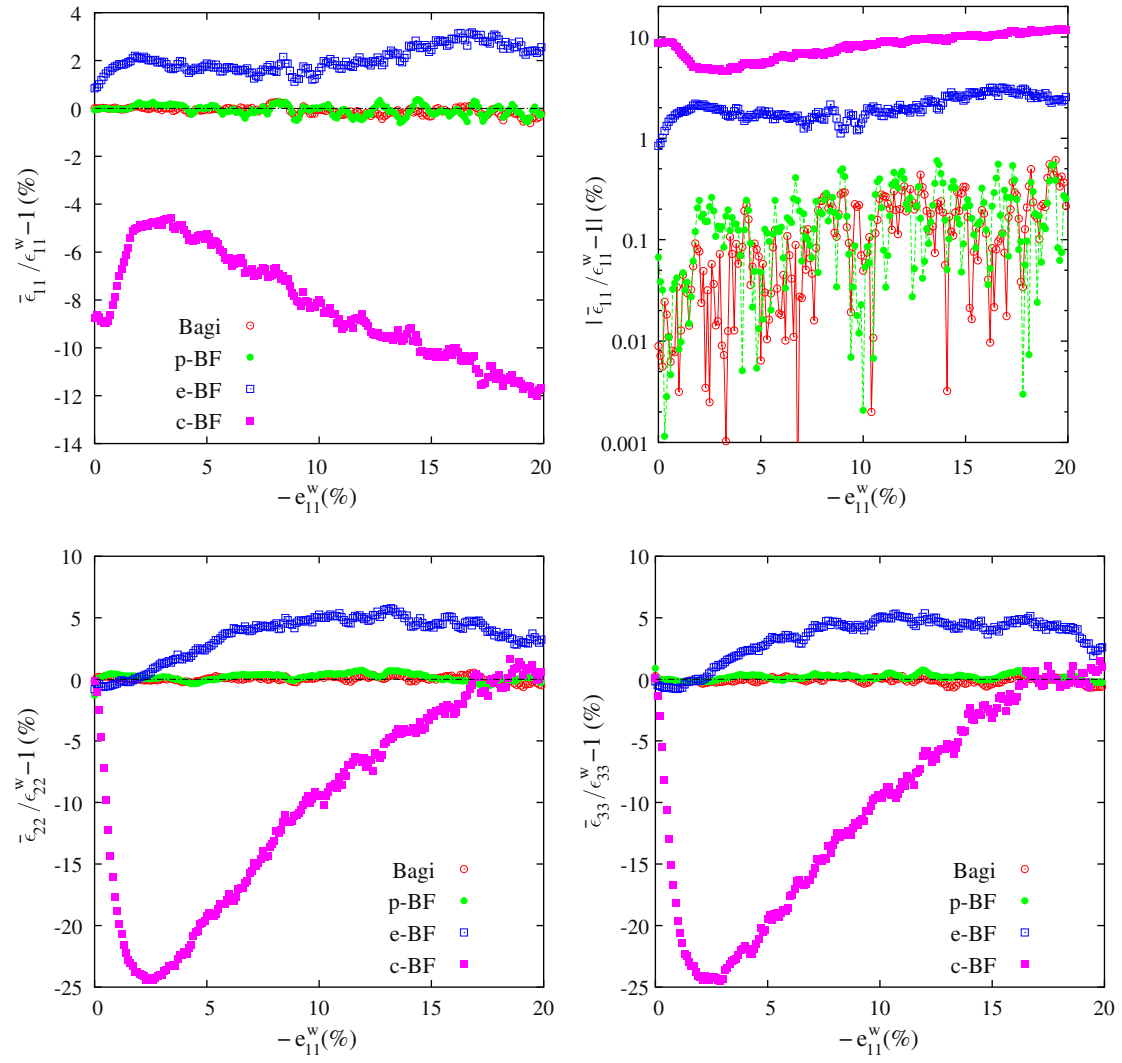

Fig. 6. Triaxial loading: deviation of the axial $\bar{\epsilon}_{11}$ (top) and lateral, $\bar{\epsilon}_{22}$ and $\bar{\epsilon}_{33}$ (bottom left and right, respectively), components of the different strains from the wall strain ϵ^w_{ij}. Linear scale (top left) and semi-log scale (top right) are shown. The latter allows for the identification of the scale of the deviation for the different strains.

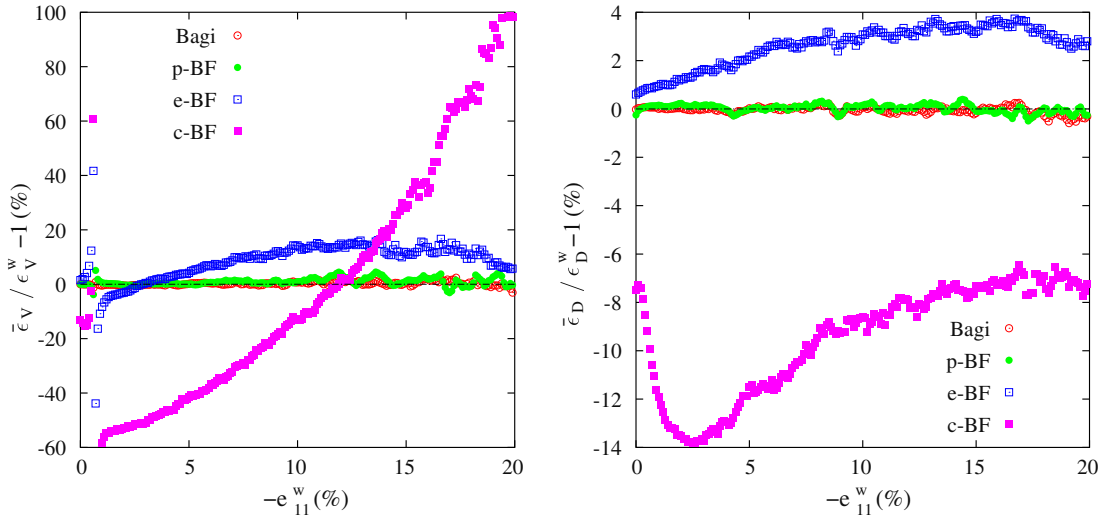

Fig. 7. Triaxial loading: deviation of the normalized volumetric strain $\bar{\epsilon}_V \equiv \mathrm{tr}\,\bar{\epsilon}_{ij}$ (left) and deviatoric strain $\bar{\epsilon}_D \equiv \bar{\epsilon}_{11} - \bar{\epsilon}_{22}$ (right) from macroscopic deformations.

In order to study the size effect, the 'reduced' system, i.e. the system formed by the M particles inside the 'reduced' volume V^*, with size $L_x \times L_y \times L_z$, is first uniformly divided into n^3 non-overlapping cells of equal size: $L_x/n \times L_y/n \times L_z/n$ and volume $V_{\text{cell}} = V^*/n^3$. In the following, the index n will uniquely characterize a given division of the system. The strain tensor ϵ_{ij}^a is then calculated for each cell a, using the Bagi and the particle-based best-fit formulations. These formulations were selected since, as shown in the previous section, they are the most accurate for describing the macroscopic deformation of the system.

The Bagi strain of a given cell a is calculated by taking the contributions of those tetrahedra with centroids inside the cell (using Eqs. (4) and (5)). The particle-based strain is directly calculated from those particles inside cell a.

After calculating the local strain tensor in each cell, two different strain averaging methods have been investigated: these are called 'V_{cell}-averaging' and 'N_{cell}-averaging'.

With 'V_{cell}-averaging', we calculate the mean strain $\langle \epsilon_{ij} \rangle_{\overline{P}} \equiv (\overline{P}/M) \sum_{a=1}^{a=n^3} \epsilon_{ij}^a$, and the standard deviation S_{ij}^{ϵ} of the strain distribution from those n^3 cells with equal volume, where $\overline{P} = M/n^3$ corresponds to the mean number of particles in each cell. However, due to the random distribution of particles in the system, equal-volume cells, corresponding to a given division n of the system, may not contain the same number of particles. Vice versa, cells with the same number of particles may correspond to a different division n.

This observation is the basis of the second averaging method, which will be called 'N_{cell}-averaging'. Here, all possible divisions of the system into n^3 non-overlapping equal-sized cells are performed, i.e. from $n = 1$ (only one cell) to $n = \mathrm{int}\left(\sqrt[3]{M}\right)$ (M cells, as many as the number of particles inside the 'reduced' volume). Next, those cells with the same number P of particles are grouped and for each group, we calculate the mean $\langle \epsilon_{ij} \rangle_P$ and standard deviation S_{ij}^{ϵ} of the strain distribution.

Fig. 8 shows the size effect on the axial strain component $\bar{\epsilon}_{11}$ resulting from the equal-volume V_{cell}-averaging of the Bagi and the particle-based best-fit formulations (symbols (○) and (●), respectively). The equal-particle-number N_{cell}-averaging of the

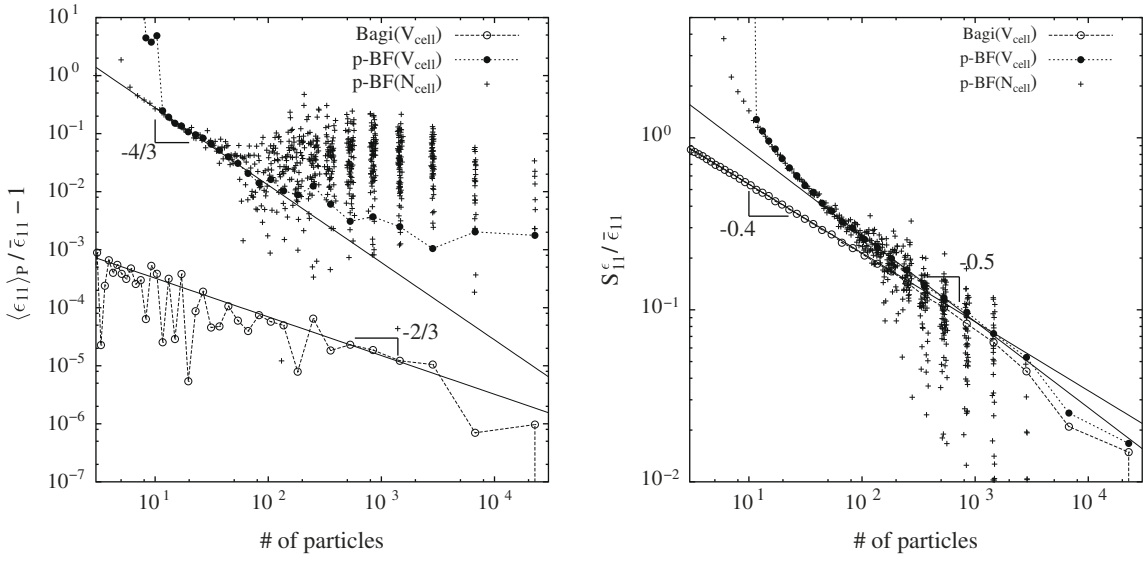

Fig. 8. Influence of the size of the averaging volume (in terms of the number of particles) on the convergence of the normalized average axial strain $\langle \epsilon_{11} \rangle_P / \bar{\epsilon}_{11}$ (left), and its fluctuation $S_{11}^{\epsilon} / \bar{\epsilon}_{11}$ (right), toward their mean-field values. Symbols represent the values obtained, in the case of Bagi, from V_{cell}-averaging (○), and, in the case of the particle-based best-fit strain (p-BF), from V_{cell}-averaging (●) and N_{cell}-averaging (+). Lines correspond to power-law scalings.

particle-based strain is also shown (symbols (+)). In Fig. 8, symbols (+) correspond to slightly different numbers of particles, although they appear clustered due to the employed logarithmic scale.

As expected, deviations from the mean-field value are larger for smaller volumes (number of particles). In particular, for the best-fit strain (p-BF) the size effect on the mean strain is three orders of magnitude larger for small volumes (Fig. 8, left). This is due to the intrinsic non-additivity of the best-fit formulation, see Eq. (17), which hence implies a size dependence. On the contrary, the Bagi strain is volume-additive, although in Fig. 8 (left) there is a small size dependence since the total volume of those tetrahedra corresponding to different cells may be slightly different (note that the Bagi strain is tetrahedron-based).

For very few particles (roughly less than 10) the mean best-fit strain arising from the V_{cell}-averaging increases sharply by more than five orders of magnitude above the mean-field value (not directly visible in Fig. 8). However, after performing the N_{cell}-averaging it is possible to determine that this increase is due to the fact that there are few cells with around 4–5 particles (see symbols (+) in Fig. 8, left), for which the best-fit method is not reliable anymore.

Furthermore, there seems to be a power-law scaling in the convergence behavior of the normalized mean axial strain $\langle\epsilon_{11}\rangle_P/\bar{\epsilon}_{11} - 1$ as function of the number of particles P, for both Bagi and the particle-based best-fit strains, with exponents $-2/3$ and $-4/3$, respectively. However, we do not have a physical interpretation for these exponents.

Regarding the size effect on the strain fluctuations S^{ϵ}_{ij} (Fig. 8, right), as expected, they also increase for decreasing volumes. In particular, for the Bagi strain, they scale as a power law with exponent -0.4, which is close, but clearly not equal, to the exponent $-1/2$ predicted by the Central Limit Theorem for independent random variables. In the case of the best-fit strain, there is a sharp increase in the fluctuations for about 10 particles, which, after separating the contributions of the cells based on their number of particles (by means of the N_{cell}-averaging), it appears to diverge at about four particles. For larger volumes, the scaling of the fluctuations in the best-fit strain seems to agree to that predicted by the Central Limit Theorem, i.e. as the inverse square root of the number of particles (Fig. 8, right).

Finally, although the V_{cell}-averaging works well for the Bagi strain, for a proper analysis of the best-fit strain, both averaging methods are needed. For small averaging cells (roughly less that 10^2 particles per cell) the N_{cell}-averaging is more suitable, while for larger cells, the V_{cell}-averaging leads to less scattered results (Fig. 8).

5. Discussion

In this study, we have presented and discussed four three-dimensional micro-mechanical strain formulations, the equivalent continuum Bagi strain (Bagi, 1996) and three best-fit strain formulations: particle-based (ITASCA, 1999), contact-based (Liao et al., 1997; Cambou et al., 2000) and edge-based (Cambou et al., 2000). From their comparison with the macroscopic three-dimensional strain, obtained from DEM simulations of isotropic and triaxial deformation of a polydisperse assembly of frictional spheres, we found that the Bagi and the particle-based best-fit strains are equally good at describing the micro-mechanical deformation of the granular system. For large averaging volumes, both are able to reproduce the macroscopic strain within a 1–2% accuracy. For small averaging volumes, Bagi's strain formulation is superior.

Regarding the other two best-fit formulations, contact and edge-based, the latter has a deviation from the macroscopic deformation below 5% (the deviation of the former one is as much as 25% for the lateral strain component $\bar{\epsilon}_{22}$).

From these results, we emphasize the following aspects. Although the particle-based best-fit strain is able to reproduce the macroscopic deformation equally well as the much more complex Bagi strain, there is a crucial difference between them. On the one hand, the best-fit strain is very simple since it is formulated in terms of particles, not contacts, and thus does neither involve the contact relative displacement nor the complexities associated with the geometrical description of the contact deformation, encoded in Bagi's complementary area vectors (Bagi, 1996) or Satake's contact-cell area vectors (Satake, 2004). On the other hand, this very characteristic makes the best-fit strain unsuitable for further, and fundamental, micro-mechanical connections to the micro-mechanical stress (described in terms of contact forces), which is an important goal of the micro-mechanical description of granular systems. Therefore, the Bagi formulation has a key theoretical advantage for a possible micro-mechanically based constitutive relation. The particle-based best-fit formulation is more suitable for numerical post-processing of results of DEM simulations.

From the micro-mechanical point of view, the Delaunay tessellation is frequently used as the structural basis for the construction of micro-mechanical strains (Bagi, 1996; Satake, 2004; Tordesillas et al., 2008). In contrast, the micro-mechanical stress formulation equation (9) is based only on the contact subnetwork. This difference in the structural basis of both tensors yields several drawbacks in the quest for the formulation of constitutive relations connecting them. Therefore, the strain should ideally be formulated in terms of the real contact subnetwork only. However, this ideal situation is so far only possible in very few cases, all of them in two dimensions, where the real contact network forms a polygonal set that tessellates the surface (Kruyt and Rothenburg, 1996; Kuhn, 1999; Kruyt, 2003). In contrast, for the three-dimensional case, the structure of the contact network is highly complex and there is no standard tessellation method for this problem (except for crystal lattice configurations).

Finally, the fact that the edge-based best-fit strain is an approximation of the Bagi strain, and clearly is less accurate, gives considerable weight to the idea that indeed, the strain of Bagi for three-dimensional granular assemblies has fundamental advantages with respect to other three-dimensional strain formulations. In particular, it seems that the Delaunay tessellation, with its (sub)set of *virtual* contacts that do not contribute to the force network, is at the core of a meaningful micro-mechanical strain definition.

Acknowledgements

The authors thank K. Bagi (Department of Structural Mechanics, Budapest University of Technology and Economics, Budapest, Hungary) for valuable discussions.

O.D. and S.L. acknowledge support from the research programme of the "Stichting voor Fundamenteel Onderzoek der Materie (FOM)", which is financially supported by the "Nederlandse Organisatie voor Wetenschappelijk Onderzoek (NWO)" (Project No. 03PGM15).

Appendix A. The complementary area vector

Using the fact that the sum of all area-vectors of the closed surface enclosing T_e tetrahedra equals zero, we have

$$\sum_{t=1}^{T_e} \mathbf{b}^{q_t} = -\sum_{t=1}^{T_e} \mathbf{b}^{p_t}. \tag{26}$$

Using Eq. (26), the definition of the complementary area vector equation (8) can be simplified to

$$\mathbf{d}^e \equiv \frac{1}{6}\sum_{t=1}^{T_e}\mathbf{b}^{q_t}. \tag{27}$$

Note that in general $\mathbf{d}^e$ is not parallel to $\mathbf{l}^e$.

Multiplication by the unit vector $\mathbf{e}_d^e \equiv \mathbf{d}^e/|\mathbf{d}^e|$, leads to the norm

$$|\mathbf{d}^e| \equiv \frac{1}{6}\sum_{t=1}^{T_e}\mathbf{b}^{q_t}\cdot\mathbf{e}_d^e. \tag{28}$$

Taking into account that $\mathbf{b}^{q_t}\cdot\mathbf{e}_d^e$ is the projected area of the surface element $\mathbf{b}^{q_t}$ (Fig. 2) into the plane perpendicular to $\mathbf{d}^e$, the norm of the complementary area vector for one edge $|\mathbf{d}^e|$ has a well-defined geometrical meaning: it is 1/6 the area of the projected (non-planar) polygonal surface formed by the centres of all particles that are simultaneously neighbors of p and q (see Fig. 9). Therefore, $\mathbf{d}^e$ contains information about the distribution of particles around a given edge e.

Appendix B. Edge-based best-fit strain as an approximation of Bagi's strain

Here, a connection between the edge-based best-fit strain as an approximation of Bagi's strain is investigated. This connection involves additional assumptions, primarily the co-linearity of The complementary area vector and the branch vector.

The complementary area vector $\mathbf{d}^e$ and the branch vector $\mathbf{l}^e$ are co-linear when

$$\mathbf{d}^e = \alpha\mathbf{l}^e. \tag{29}$$

The constant α can be determined from the geometrical constraint equation (11). Taking the trace of both sides of Eq. (11), and substituting $\mathbf{d}^e$ by $\alpha\mathbf{l}^e$,

$$3V = \sum_e \mathbf{l}^e\cdot\mathbf{d}^e = \alpha\sum_e \mathbf{l}^e\cdot\mathbf{l}^e = \alpha E\left\langle l_e^2\right\rangle_e \tag{30}$$

gives

$$\alpha = \frac{3V/E}{\left\langle l_e^2\right\rangle_e}. \tag{31}$$

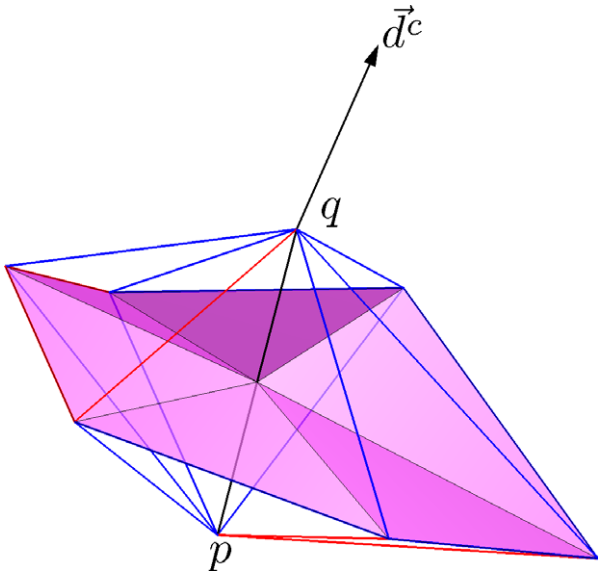

Fig. 9. The complementary area vector $\mathbf{d}$ is 1/6 times the area-vector of the (non-planar) polygonal surface (in magenta) defined by the position of the nearest neighboring particles (vertices) of the edge pq (black line), and the midpoint of the branch vector $\mathbf{l}^{pq}$ (see also Fig. 3). (For interpretation of the references to color in this figure legend, the reader is referred to the web version of this paper.)

For a random granular packing, we have checked that the branch vectors $\mathbf{l}^e$ of Delaunay edges are isotropic on average (data not shown). Hence, the extended fabric tensor, $\mathscr{F}^*_{ik} \equiv \langle l_i^e l_k^e\rangle_e$, is also isotropic with trace $\mathrm{tr}\,\mathscr{F}^* = \left\langle l_e^2\right\rangle_e$, where the average is over all edges. Note that the corresponding fabric tensor based on contacts is generally not isotropic. This leads to

$$\mathscr{F}^*_{ik} = \frac{\left\langle l_e^2\right\rangle_e}{3}\delta_{ik}. \tag{32}$$

Therefore, Eq. (22) becomes

$$\bar{\epsilon}_{ij} = 3\frac{\left\langle \Delta u_j^e l_i^e\right\rangle_e}{\left\langle l_e^2\right\rangle_e}. \tag{33}$$

On the other hand, after substituting Eqs. (29) and (31) into the expression for the Bagi strain, Eq. (7), one has

$$\bar{\epsilon}_{ij} = \frac{E}{V}\left\langle \Delta u_i^e d_j^e\right\rangle_e, \tag{34}$$

$$= \alpha\frac{E}{V}\left\langle \Delta u_i^c l_j^e\right\rangle_e, \tag{35}$$

$$= 3\frac{\left\langle \Delta u_i^e l_j^e\right\rangle_e}{\left\langle l_e^2\right\rangle_e}, \tag{36}$$

which is identical to Eq. (33).

Hence, it has been shown that the edge-based best-fit strain is an approximation of the Bagi strain, under some additional assumptions.

References

Bagi, K., 1996. Stress and strain in granular assemblies. Mech. Mater. 22, 165–177.

Bagi, K., 2006. Analysis of microstructural strain tensors for granular assemblies. Int. J. Solids Struct. 43, 3166–3184.

Bagi, K., 2006. Discussion of the paper Tensorial form definitions of discrete mechanical quantities for granular assemblies. Int. J. Solids Struct. 43, 2840–2844.

Cambou, B., Dubujet, F., Emeriault, F., Sidoroff, F., 1995. Homogenization for granular materials. Eur. J. Mech. A/Solids 14 (2), 255–276.

Cambou, B., Chaze, M., Dedecker, F., 2000. Change of scale in granular materials. Eur. J. Mech. A/Solids 19, 999–1014.

Cundall, P.A., Strack, O.D.L., 1979. A discrete numerical model for granular assemblies. Géotechnique 29, 47–65.

Drescher, A., de Josselin de Jong, G., 1972. Photoelastic verification of a mechanical model for the flow of a granular materials. J. Mech. Phys. Solids 20, 337–351.

Drummen, M. 2006. DEM simulations and theory of the HCP. M.Sc. Thesis, Department of Chemical Engineering, Technological University of Delft, Delft, The Netherlands.

Goldhirsch, I., Goldenberg, C., 2005. Continuum mechanics for small systems and fine resolutions. In: Rieth, M., Schommers, W. (Eds.), Handbook of Theoretical and Computational Nanotechnology. American Scientific Publishers, Stevenson Ranch, CA, pp. 1–58.

ITASCA, 1999. Particle flow code in two dimensions. Users Manual: Theory and Background. ITASCA, Minneapolis, MN, pp. 3.11–3.13.

Kruyt, N.P., 2003. Statics and kinematics of discrete Cosserat-type granular materials. Int. J. Solids Struct. 40, 511–534.

Kruyt, N.P., Rothenburg, L., 1996. Micromechanical definition of strain tensor for granular materials. ASME J. Appl. Mech. 118, 706–711.

Kuhn, M.R., 1999. Structured deformation in granular materials. Mech. Mater. 31, 407–429.

Lätzel, M., Luding, S., Herrmann, H.J., 2001. From discontinuous models towards a continuum description. In: Vermeer, P.A., Diebels, S., Ehlers, W., Herrmann, H.J., Luding, S., Ramm, E. (Eds.), Continuous and Discontinuous Modelling of Cohesive Frictional Materials. Springer, Berlin, pp. 215–230.

Liao, C.-L., Chan, T.-C., 1997. A generalized constitutive relation for a randomly packed particle assembly. Comput. Geotech. 20 (3/4), 345–363.

Liao, C.-L., Chang, T.-P., Young, D.-H., Chang, C.S., 1997. Stress–strain relationship for granular materials based on the hypothesis of best fit. Int. J. Solids Struct. 34, 4087–4100.

Liu, Y., Snoeyink, J., 2005. A comparison of five implementations of 3D Delaunay tessellation. Comb. Comput. Geom. 52, 439–458.

Luding, S., 2008a. Cohesive frictional powders: contact models for tension. Granul. Matter 10, 235–246.

Luding, S., 2008b. The effect of friction on wide shear bands. Particul. Sci. Technol. 26, 33–42.
Satake, M. 2002. Micro-mechanical definition of strain tensor for granular assemblies. In: Smyth, A. (Ed.), Proceedings of the 15th ASCE Engineering Mechanics Conference.
Satake, M., 2004. Tensorial form definitions of discrete-mechanical quantities for granular assemblies. Int. J. Solids Struct. 41, 5775–5791.
Tordesillas, A., Walsh, S.D.C., Muthuswamy, M., 2008. The effect of local kinematics on the local and global deformations of granular systems. Math. Mech. Solids. doi:10.1177/1081286507089844.